Characterization of a precast hemp concrete. Part I: Physical and thermal properties

Billy Seng, Camille Magniont, Sylvie Lorente

Characterization of a precast hemp concrete. Part I: Physical and thermal properties

Billy SENG, Camille MAGNIONT, Sylvie LORENTE

LMDC, Université de Toulouse, UPS, INSA, 135 Avenue de Rangueil, 31077 Toulouse

cedex 04, France

Corresponding author: Camille MAGNIONT

e-mail: camille.magniont@insa-toulouse.fr

Abstract

Hemp concrete is seen as a possible solution for addressing the energy, health and comfort issues of sustainable buildings, thanks to its hygrothermal properties and environmental qualities. This paper aims to determine the physical and thermal properties of an industrial prefabricated hemp concrete block based on hemp shiv and a lime-metakaolin binder. When available, distinct measurement methods were applied and confronted on this precast material in order to evaluate the impact of the experimental procedure on the results. Concerning air permeability, the present study shows that a measurement method initially intended for regular concrete can be adapted to the specific behaviour of highly permeable material such as hemp concrete. The thermal conductivity was measured with a guarded hot plate and a hot wire. Hot wire measurements on different moist states of the material allowed the self-consistent scheme to be applied for the evaluation of the thermal conductivity as a function of the humidity. Two direct measurement methods, differential scanning calorimetry (DSC) on the components and use of a Calvet calorimeter on the hemp concrete, and one indirect method, through effusivity measurement, were adopted for evaluating the specific heat capacity of the material. The original method proposed using DSC was shown to be as accurate as direct calorimetric measurement. The direct measurement methods gave similar results while the indirect one led to a much lower value. A comprehensive analysis of the measurement values available in the literature on hemp concretes confirmed this trend.

This first paper highlights the significant influence of the testing method on the determination of the thermal properties of a precast hemp concrete, especially on the heat capacity measurement. This result emphasizes the need for a large inter-laboratory experimental campaign, applied to bio-aggregate based concrete, in order to form the basis of recommendations for adequate physical and thermal characterization methods for these bio-

based building materials. A second part of this study will investigate the hydric properties of the same material.

Keywords: Thermal properties, specific heat capacity, hemp concrete, air permeability.

1. Introduction

Nowadays, the environmental and energy context encourages building constructors and users to seek more and more environmentally friendly solutions. In France, the building sector is responsible for 45% of the final energy consumption (Service de l'observation et des statistiques (SOeS), 2016) and 20% of the greenhouse gas emissions (Service de l'observation et des statistiques (SOeS), 2017). Thus, buildings need to be made more energy efficient and their global environmental impact should also be reduced – but without ignoring the increasing demands for indoor comfort throughout a building's lifetime. The "$E^{+}C^{-}$" label, which paves the way for future French regulations in this area, improves the energy requirements while also considering the carbon footprint (Ministère de la transition écologique et solidaire and Ministère de la cohésion des territoires, 2017).

Indeed, increasing buildings energy efficiency increases the relative part of the construction materials and systems in the environmental impact of the building. Thus, building materials now appear to be a key factor in the global footprint (Blengini and Di Carlo, 2010; Buyle et al., 2013). In this context, there is renewed interest in bio-based building materials. These materials contain biomass, i.e. plant or, more rarely, animal (e.g. wool) components and can thus store carbon for the lifespan of the construction. Compared to standard materials, they generally need less embodied energy. A large variety of plants (wood, hemp, flax, straw, bamboo, rattan, reeds, etc.) (Jones and Brischke, 2017) can be used as raw material depending on the location of the project and the existence of plentiful local supplies of such biomaterials constitutes one of their main environmental benefits. They can be used directly as bulk raw material or in various processed forms (fibre, panel, bio-aggregate concrete, etc.). Furthermore, thanks to the porous structure of the plants and even of the overall material in some cases, bio-based materials have efficient insulating and hygroscopic properties, which help to improve the thermal comfort of the building during its use (Latha et al., 2015). Such

materials have the ability to absorb and desorb humidity in the air. Thus they act as moisture buffering materials and have a damping effect on the variations of relative humidity (RH)(Rahim et al., 2016c). Avoiding extreme values of humidity helps to maintain indoor comfort (Fang et al., 1998), limits the development of micro-organisms (Gradeci et al., 2017) and their consequent health issues, and contributes to the durability of the material (Viitanen et al., 2010).

Among the tremendous choice of bio-materials for construction, hemp concrete, a lightweight bio-aggregate-based concrete, has excellent agronomic features, good hygroscopic properties and is self-supporting. Because of these qualities, professional rules for hemp concrete were laid down in 2007 in France (Association Construire en chanvre and Collectif FFB, 2007), and have allowed the development of this construction technique and the concomitant development of scientific studies on this material.

Hemp concrete is composed of hemp shiv particles, as the plant aggregates, and a binder, generally based on lime in order to maintain the hygroscopic properties. Hemp shiv is the woody core of the hemp stalk obtained through defibration by a mechanical breaking process. Hemp has the particularity of needing very little fertilizer and water compared to other crops. It grows quickly and it is more resistant to biological decay than many other plants (Shea et al., 2012). With regards to the binder, different formulations can be used, in most cases based on hydraulic or aerial lime and possibly including a pozzolanic component or other additives. Different mixing ratios of the components can be chosen, leading to different uses: as wall filling material, roof or floor insulation, or even indoor plaster. In wall configuration, the material must be used in complement to a post and beam structure because its mechanical properties do not allow this material to be load bearing (Arnaud and Gourlay, 2012; Walker and Pavía, 2014). Hemp concrete can be cast, sprayed on temporary or permanent shuttering or pre-fabricated in blocks. The latter method has the advantage of avoiding long drying time

of the material, which, when it is built in situ, can reach several months (Glouannec et al., 2010; Walker and Pavía, 2012). Therefore pre-fabrication is more suited to the time constraints of modern construction.

In this context, this series of two papers focuses on the physical and hygrothermal characterization of a pre-fabricated hemp concrete block manufactured by the SEAC company and resulting from previous research works on the material formulation carried out as a joint effort by SEAC and the laboratory LMDC (Escadeillas et al., 2010; Gazagnes et al., 2010). The characteristics of this material are determined so as to be able to simulate its hygrothermal behaviour in a further study by using a heat and moisture model presented by Seng et al. (2017) and to confront these results with experimental data obtained at wall scale from a bi-climatic chamber (Vu et al., 2015).

In the literature, hemp concrete has been studied since the 2000's: experimentally, with the characterization of its hygrothermal properties, and numerically, with the prediction of the temperature and humidity inside the material and in the surrounding air, using the hygrothermal properties in heat and moisture models. However, no internationally standardized method exists for the experimental hygrothermal characterization of such materials (very permeable and hygroscopic). Previous studies have been based on the transposition of existing standard protocols from mineral-based to bio-based materials or on the development of specific protocols. As stated by various authors (Delgado et al., 2013; Plagge et al., 2007), the usual experimental characterization sometimes shows a limited ability to describe the complexity of the behaviour of such material under heat and moisture stresses. So, one current issue to be investigated is the interdependence of heat and moisture phenomena, i.e. the fact that the thermal properties depend on the humidity and the hydric properties depend on the temperature.

The main physical properties are the material density and the open/closed porosity. A good knowledge of the structure helps to understand and explain the thermal and hydric properties. Depending on the formulation, the density of hemp concrete can vary. The porosity is high compared to that of standard building materials, around 70 to 90%. Benfratello et al. (2013) and Collet and Pretot (2014) built different hemp concretes with different methods and formulations and found densities from 377 to 611 $kg.m^{-3}$. The total porosities found by the first author range from 72 to 85%. With regards to the physical properties, we can also consider the air permeability. However, to our knowledge, only a single air permeability characterization has been published in the literature. Cerezo (2005), evaluated the material air permeability at around 10^{-9} m^2, which is close to the air permeability of a mineral wool.

The thermal conductivity of hemp concrete is its most extensively studied property to date (Benfratello et al., 2013; Collet and Pretot, 2014; de Bruijn and Johansson, 2013; Rahim et al., 2016a; Walker and Pavía, 2014) but the impacts of different parameters have also been investigated: density, type of binder, mix ratio, anisotropy, level of compaction, and humidity (relative humidity or water content). Depending on these parameters, most of the measurements of thermal conductivity range from 0.09 to 0.14 $W.m^{-1}.K^{-1}$. The thermal conductivity seems to have a linear relationship with density (0.06 to 0.18 $W.m^{-1}.K^{-1}$ for densities from 200 to 800 $kg.m^{-3}$ according to Cerezo (2005)), temperature (0.123 to 0.128 $W.m^{-1}.K^{-1}$ for a temperature between 10 and 40 °C (Rahim et al., 2016a)) and moisture content, where Collet and Pretot (2014) and Gourlay et al. (2017) have reported that its value can increase by 15-20% when the moisture content varies between 0 and 4%. Various techniques have been applied to measure this property: guarded hot plate, hot wire, hot box, or hot plate. The first two were used in the present study. Other thermal properties have been investigated, but to a lesser extent, such as the thermal diffusivity or, even more rarely, the specific heat capacity or the effusivity. In particular, there is a notable dispersion, from 770 to

1560 $J.kg^{-1}.K^{-1}$, of the specific heat capacities measured by Collet (2004), Evrard (2008), and Gourlay et al. (2017). The specific heat capacity of the prefabricated hemp concrete studied in the present study was measured using three distinct techniques: a direct measurement employing differential scanning calorimetry (DSC) on each component of the hemp concrete, a direct measurement with a Calvet calorimeter on crushed composite samples, and an indirect determination from the measurement of thermal effusivity and conductivity.

The work described in this first paper aimed to measure the physical and thermal properties of prefabricated hemp concrete: density (apparent and true density), porosity (open and total porosity), air permeability, and thermal properties (thermal conductivity, effusivity and specific heat capacity). All the measurements were performed on samples directly extracted from the industrially produced bricks. Therefore, the large variability of performance, often reported in the literature for the manual casting method, was limited. The second objective of the present study was to investigate the impact of the experimental methods and protocols on the assessed performances. When possible, different methods were used for measuring the same parameter and the results were compared with those found in the literature, where "homemade" protocols or non-specific standards were often applied. For the air permeability measurement in particular, a measurement protocol for highly permeable building materials is proposed, based on the implementation of a concrete permeameter (CEMBUREAU).

2. Material and methods

2.1. Material

The material we are interested in came from SEAC, a company specializing in concrete walls and floors, and also developing sustainable construction materials. The design of the brick was the result of previous research works on the material formulation, performed jointly by SEAC and LMDC, and which led to two patents for a vibro-compacted precast hemp concrete

(HC) (Escadeillas et al., 2010; Gazagnes et al., 2010). The precast block was made of hemp shiv aggregates and an innovative lime-metakaolin (LM) binder (Dinh et al., 2015; Magniont et al., 2012).

The hemp shiv aggregates are ligneous particles extracted from the core of hemp stems (*Cannabis sativa*) through an industrial defibration process using mechanical breaking. The particles are then dusted and calibrated. The pozzolanic matrix was made of lime and metakaolin, produced by flash calcination of kaolinite at 700 °C, and mainly composed of amorphous silicon-aluminates and quartz.

The precast block, previously cured in the prefabrication plant, can be used directly on a construction site without a long drying time. However, the material is not a load-bearing construction product, and it needs a framework such as a post and beam structure. At present, the bricks are intended to be used as filling material only. In Figure 1, two types of block are presented. Type B block, with an empty space, allows for the passage of the load-bearing structure. In this study, we focus on type A bricks.

Figure 1: Type A brick (left) and type B brick (right) for framework post

The brick dimensions were measured with a vernier caliper on 2 bricks selected at random: the length was 50.75±0.95 cm, the depth was 19.90±0.09 cm and the height was 20.28±0.24 cm. Some thickness discrepancies could be noted (Figure 2) between the six vertical slabs on one hand, and between the top and bottom part of each slab on the other. These differences

can be explained by the vibro-compaction fabrication process, which generates vertical segregation.

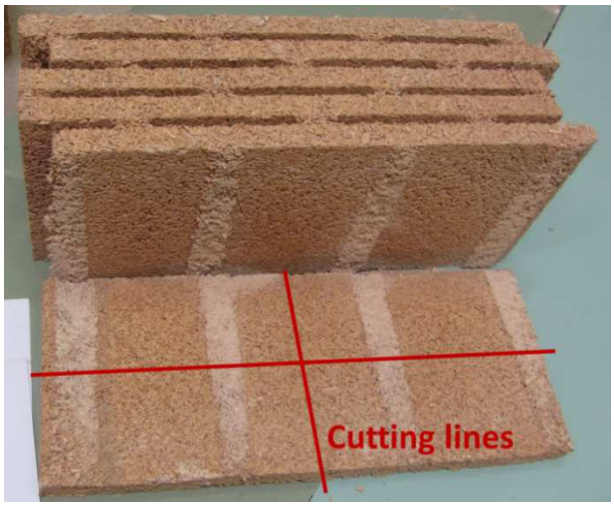

Figure 2: Sampling for apparent density study

Samples were cut from the slabs of the bricks with a circular bridge saw for rectangular samples and with a core drilling machine for cylindrical samples. In order to avoid shredding, the cutting lines on the samples were soaked with water prior to the cutting process. All the samples were taken in such a way that the studied transfer was in the same direction, i.e. along the horizontal axis of the brick, even for capillary water absorption. The dimensions of the samples are given in Table 1. The components, i.e. hemp shiv and binder, were also studied for some parameters. The hemp shiv used in this study was the same as that used for the production of the hemp concrete bricks (Cannahabitat from Agrofibre) and the binder was reproduced in the laboratory with a water to binder ratio of 1 from the industrial formulation.

Studied parameter	Geometry – Dimensions	Precision
Apparent density	Rectangular 25x10x2.5 cm^3	10^{-2} g
Density of the solid	Powder 80 µm	10^{-3} g
Open porosity	Rectangular 25x10x2.5 cm^3	10^{-2} g
Air permeability	Cylindrical: radius=11 cm, height=2.5 cm	10^{-3} g
Thermal conductivity (Guarded hot plate (GHP) & Hot wire))	GHP: Rectangular 15x15x2.5 cm^3 Hot wire: Rectangular 25x10x2.5 cm^3	10^{-2} g
Specific heat capacity (Differential Scanning Calorimetry (DSC))	Powder 80µm	10^{-3} g
Specific heat capacity (Effusivity)	Rectangular 25x10x2.5cm^3	10^{-2} g
Specific heat capacity (Calorimeter)	Crushed sample from quartering, m ≈5 g	-

Table 1: Balance information for mass stabilization monitoring and experimental study

2.2. **Methods**

For most experiments, the samples had to be considered first in the dry state. Drying was performed in a climatic chamber at 50 °C, 10% RH for the apparent density study, and in a laboratory oven at a temperature of 50 °C for the other experiments: density of the solid, thermal conductivity, and specific heat capacity. The preparation of the samples was considered to be achieved when the sample mass change was less than 0.1% between two weighings at least 24 hours apart (5% for the vapour permeability study). After drying, the samples were stored at ambient temperature in a desiccator or a hermetic box with silica gel for the thermal property measurements. For the air permeability, the samples were kept at ambient conditions.

For the measurement of the density of the solid (hemp shiv, binder and hemp concrete) and for the specific heat capacity measurement with differential scanning calorimetry, the material

had to be in powder form. All the materials were ground at 80 µm. A centrifugal mill was used for the hemp and the hemp concrete brick, previously broken into small pieces. For the HC brick, homogeneous samples were obtained by quartering on a small monolithic HC. An agate mortar and a sieve were used for the binder.

The details of the mass stabilization monitoring are presented in Table 1. If a different apparatus was used for the experiment, it is specified in the corresponding subsection.

2.2.1. Density, porosity and mass ratios

Three hemp concrete (HC) bricks were used for measuring the apparent density $\rho_{a,HC}$. Each slab was cut into four pieces (see Figure 2 and Table 1) and dried at 50 °C until mass stabilization. The final mass was recorded. The dimensions of the samples were measured with a vernier caliper, allowing the volume calculation and then the apparent density calculation.

The solid density of the hemp shiv aggregates (ρ_{hemp}) and the lime-metakaolin binder (ρ_{binder}), as well as of the HC brick (ρ_{HC}) were evaluated through hydrostatic weighing of 80 µm powder performed in a non-reactive solvent (Aitcin et al., 1968). For each component, three samples were studied. They were saturated and weighed in the solvent using a balance (10^{-3} g).

The solid density of the component *i* is given by Eq. (1):

$$\rho_i = \frac{m_{i,air}}{m_{i,air} - m_{sat.i,garosolve}} \rho_{garosolve} \quad (1)$$

where $m_{i,air}$ (kg) is the mass of the sample of component *i* in air (total mass of both the Erlenmeyer flask and the sample minus the mass of the flask alone in air), and $m_{sat.i,garosolve}$

(kg) is the mass of the saturated sample of component *i* immersed in the solvent (total mass of the Erlenmeyer flask and the sample minus the mass of the flask alone in the solvent).

Based on the apparent density $\rho_{a,HC}$ and the solid density ρ_{HC} of the material, it was possible to calculate the total porosity ε_{tot}, the ratio of the void volume to the total volume. It is given by Eq. (2):

$$\varepsilon_{tot} = 1 - \frac{\mathrm{V_{solid}}}{\mathrm{V}_{app}} = 1 - \frac{\rho_{a,HC}}{\rho_{HC}} \tag{2}$$

where V_{app} is the apparent volume of a sample (m^3), $\mathrm{V_{solid}}$ is the solid matrix volume (m^3).

The open porosity ε_{open} was measured on monolithic HC samples, by hydrostatic weighing in water (Eq. (3)) (AFPC-AFREM, 1997). This measurement was performed on four samples (25x10x2.5 cm^3):

$$\varepsilon_{open} = \frac{\mathrm{m_{sat.HC,air}} - \mathrm{m_{HC,air}}}{\mathrm{m_{sat.HC,air}} - m_{sat.HC,water}} \tag{3}$$

where $\mathrm{m_{sat.HC,air}}$ is the mass of vacuum saturated HC in air, $\mathrm{m_{HC,air}}$ is the mass of the dry HC sample in air and $m_{sat.HC,water}$ is the mass of the saturated sample in water.

The mass ratio x_i of the component *i* is defined in Eq. (4) by the ratio of the mass of the component *i* in a HC sample, m_i , and the total mass of the HC sample m_{HC}:

$$x_i = \frac{m_i}{m_{HC}} \tag{4}$$

The mass ratios of hemp and binder in the composite were calculated from mass and volume conservation, Eq. (5):

$$\begin{cases} x_{hemp} = (\rho_{binder} - \rho_{HC})/(\rho_{binder} - \rho_{hemp}) \\ x_{binder} = 1 - x_{hemp} \end{cases} \tag{5}$$

2.2.2. Air permeability

The gas permeability k_p (m^2) is the ability of a material to let air pass through it under a pressure difference.

The apparatus used for air permeability measurement in the present study (Figure 3) was adapted from the CEMBUREAU permeameter (Cembureau Recommendation, 1989) as the original apparatus was not designed for highly permeable material. The cylindrical sample, protected by an aluminium ring and sealed with silicone, was inserted in a permeability cell with a confinement air chamber set at 3 bars. Air coming from a pressurized bottle passed through different pressure regulators, reducing the pressure, and the flow rate was adjusted by a mass flow controller. Two different mass flow controllers were tested in order to cover the range 0-300 $mL.min^{-1}$ and the range 0-2000 $mL.min^{-1}$. A flow meter was placed upstream of the regulator in order to check the volumetric flow rate. A differential pressure gauge upstream of the sample measured the difference of pressure between the inlet pressure P_{in} and the atmospheric pressure, corresponding to the outlet pressure P_{out}. All the measurements were carried out in a room where the temperature was regulated at 21°C.

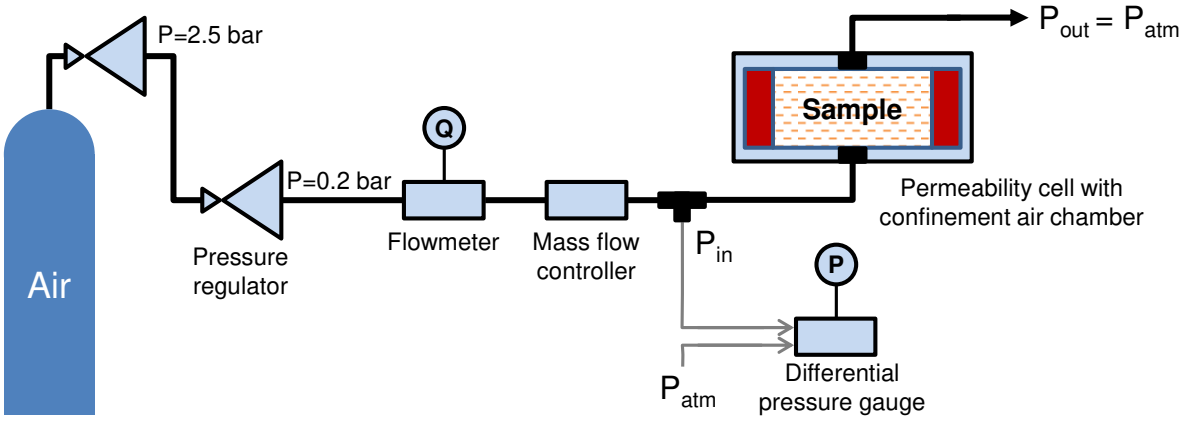

Figure 3: Scheme of the gas permeability measurement apparatus, adapted from the CEMBUREAU permeameter (Cembureau Recommendation, 1989).

Darcy's law links the air flow through a sample with the inlet pressure P_{in} and the outlet pressure P_{out}. In the case where the compressibility effect is negligible, the apparent gas permeability k_{app} is derived from this relationship (Eq. (6)):

$$k_{p,app} = \frac{\mu_{air} L Q}{A(P_{in} - P_{out})} \quad (6)$$

where μ_{air} is the air viscosity (μ_{air}=1.8 10^5 Pa.s at 21°C), L is the thickness of the sample (m), Q is the gas volumetric flow rate ($m^3.s^{-1}$), A is the cross section (m^2), P_{in} and P_{out} are respectively the absolute inlet pressure (Pa), before the sample, and the absolute outlet pressure (P_{out}=P_{atm}).

Two samples were tested. Each was formed by the assembly of two layers of hemp concrete: the contact surfaces between the two layers were sanded in order to limit the air layer between them. The thicknesses of the two samples were 4.7 and 5.2 cm and the diameters were 9.7 and 9.8 cm, respectively. Three measurements were performed on the 1st sample and four measurements on the 2nd sample, for a flow rate between 0 and 300 $mL.min^{-1}$. One additional set of measurements was performed for a flow rate in the range 300-2000 $mL.min^{-1}$.

For the sake of calibration, Eq. (6) was used to evaluate the order of magnitude of the pressure gauge. This was a challenge as almost no measurements of air permeability on hemp concrete are available in the literature. Cerezo (2005) proposed a value of 10^{-9} m^2, which corresponds to the permeability of a mineral wool. With the hypothesis of an air permeability in the range 10^{-9}-10^{-10} m^2 and a flow between 0 and 3000 $mL.min^{-1}$, a theoretical difference of pressure of up to 60 Pa was found, which allowed the sizing of the differential pressure gauge.

2.2.3. Thermal conductivity

The thermal conductivity k (W.m^{-1}.K^{-1}) is the ability of a material to conduct heat under a gradient of temperature. Two distinct methods were applied to measure thermal conductivity: a steady-state technique (guarded hot plate (GHP)) and a transient one (hot wire).

The guarded hot plate was used to measure the thermal conductivity of six parallelepipedic dry samples (15x15 cm^2 cross section) according to the NF EN 12664 standard (AFNOR, 2001). The accuracy of measurement is equal to 0.1% for temperature and lower than 1% for thickness below 90 mm. The resulting accuracy on thermal conductivity is of the order of 5%. In this measurement, based on a 1D Fourier's law, a heat transfer rate was created through the HC sample by means of two plates: a hot plate above the sample and a cold plate underneath (Figure 4). The resulting heat flux was recorded with respect to time. Insulating material around the sample limited the heat losses. The measurements were performed at average temperatures of 10 °C, 23 °C and 40 °C with a difference of 5 °C between the two plates. Steady-state was considered to have been reached when the change in conductivity was less than 1% in 90 minutes. The thermal conductivity of the dry material k_{dry} (W.m^{-1}.K^{-1}) was then calculated.

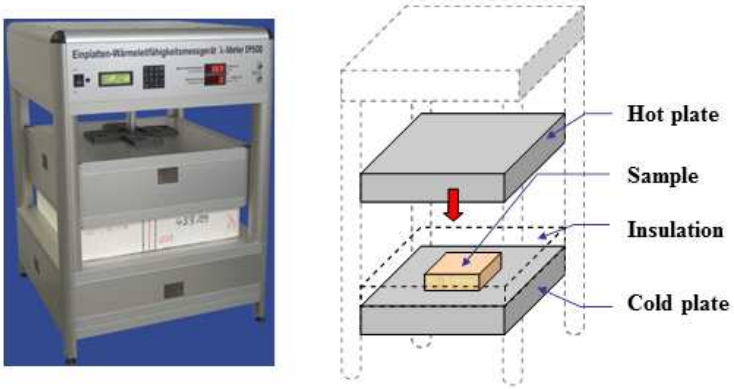

Figure 4: Guarded hot plate (GHP)

A thermal conductivimeter with a hot wire was used to measure the thermal conductivity of dry and wet samples. According to the technical specifications provided by the manufacturer, the accuracy on thermal conductivity is of 5%. The hot wire method is a transient technique in which an increase of the material temperature is measured. A linear wire, assumed to be of infinite length and negligible diameter, generates heat under the influence of an electric current. Here, the wire and the associated thermocouple were included in a Kapton probe placed between two samples of the material (Figure 5).

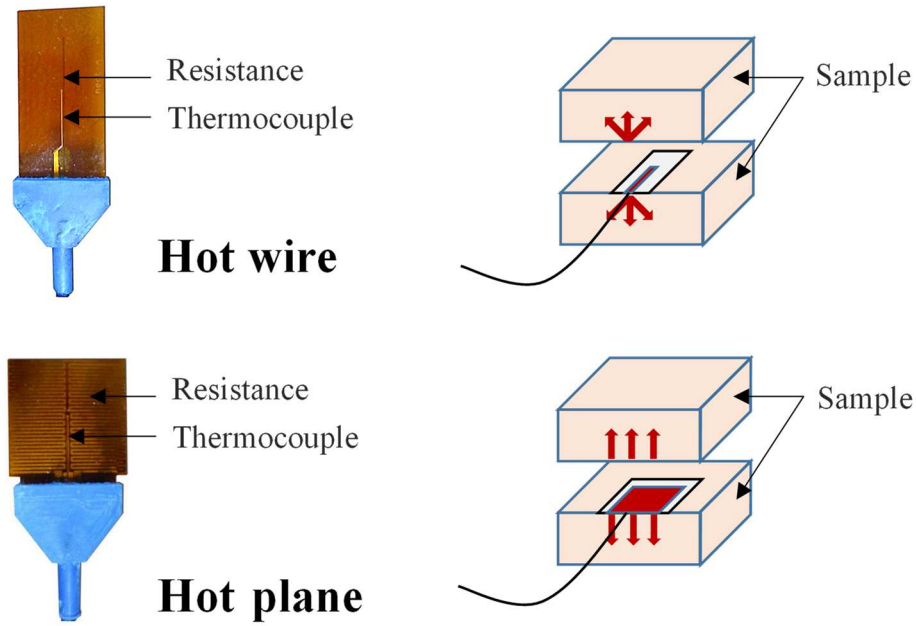

Figure 5: Hot wire and hot plane schemes

According to the work of the pathfinders Carslaw and Jaeger (1959), a simplified relation can be found between the temperature and the thermal conductivity k. It is obtained by solving the heat conduction equation in cylindrical coordinates over a sufficiently long time, assuming semi-infinite media, Eq. (7):

$$\mathrm{T(r,t)} = \frac{\mathrm{q'}}{4\pi k}\left[\ln\left(\frac{4\alpha t}{r^2}\right) - \gamma\right] \tag{7}$$

where r is the radial position of the temperature measurement (m), t is the time (s), q' is the heat per unit length ($W.m^{-1}$), α is the thermal diffusivity of the material ($m^2.s^{-1}$) and γ=0.5772156 is Euler's constant.

Between times t_1 and t_2 ($t_1 < t_2$), the temperature changes from T_1 to T_2, and:

$$T_2 - T_1 = \frac{q'}{4\pi k} \ln\left(\frac{t_2}{t_1}\right) \quad (8)$$

Hence, k can be deduced from the slope of Eq. (8). The heat per unit length, q', and the time of study were selected to obtain a sufficient increase in temperature (~10 K) and a high correlation coefficient R^2 (>0.999) when plotting the increase of temperature with time.

A total of 18 different samples (25x10x2.5 cm^3) were used. Some samples were dry, others moist, set in equilibrium at 50% and 65% RH. The wet samples were placed in rooms where the RH was controlled and the temperature set at 20 °C. The condition at 95% RH was tested. However, it was not possible to reach complete equilibrium due to the risk of mould development.

2.2.4. Specific heat capacity

The specific heat capacity c_p ($J.kg^{-1}.K^{-1}$) of a material is its ability to store thermal energy.

Three different methods were applied to measure the specific heat capacity of the hemp concrete: a direct measurement through differential scanning calorimetry (DSC) on each component of the HC (binder and hemp shiv), a direct measurement with a Calvet calorimeter on crushed composite samples, and an indirect determination by measuring the thermal effusivity, thermal conductivity and apparent density.

DSC measurements were based on standards ISO 11357-4 and ASTM E1269-11 (AFNOR, 2014; ASTM, 2011), three cycles were performed using the same thermal programme

composed of a first step at constant temperature, an increase of temperature and a final step at constant temperature (Figure 6). For each cycle, two crucibles were used. The experimental set-up is presented in Figure 7.

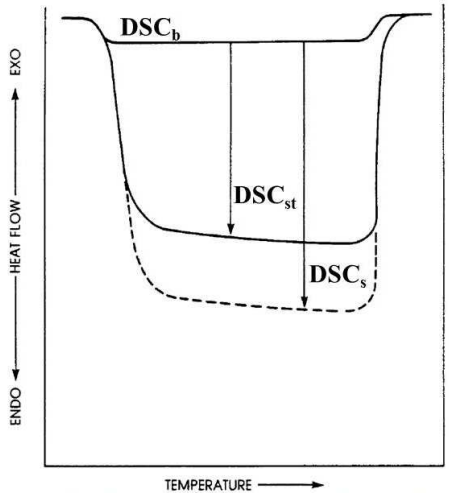

Figure 6: Typical DSC signal for blank cycle, standard cycle and sample cycle (from ASTM E1269-11) (ASTM, 2011)

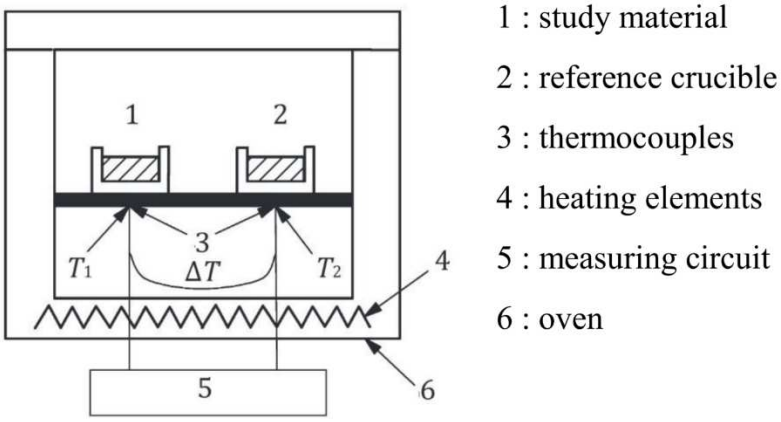

Figure 7: Scheme of the DSC system (from ISO 11357-1) (AFNOR, 2016)

One of the crucibles served as a reference and was kept empty during all the measurements. The other contained the different materials. The same crucibles were used throughout a whole

measurement, i.e. for the three cycles. The first cycle was the blank one with empty crucibles; the second one, called the "reference cycle", was performed with a sapphire sample, also referred to as the standard sample; and the last one was the "sample cycle" when the specific heat capacity of the hemp concrete sample was measured. The difference in specific heat capacity of the reference and the study crucibles led to a difference of temperature between them. The DSC signal comes from the difference of temperature between the two crucibles measured with thermocouples (µV). This difference is representative of the difference of heat flux. Starting from the physical phenomenon, Eqs. (9) to (14) detail how the value of the heat capacity c_p is obtained. From the definitions of the heat energy transferred during an increase of temperature, we have:

$$\begin{cases} m_{st} c_{p,st} dT = \delta Q_{st} & (9) \\ m_s c_{p,s} dT = \delta Q_s & (10) \end{cases}$$

where δQ_{st} and δQ_s(J) are the heat transferred to the standard crucible (sapphire) and the study crucible (material under study), respectively, for an increase of temperature dT; m_{st} and m_s (g) are the mass of the standard sample and the mass of the studied sample; and $c_{p,st}$ and $c_{p,s}$ (J.kg^{-1}.K^{-1}) are the specific heat capacity of the standard sample and the studied sample.

Dividing Eq. (10) by Eq. (9), we obtain Eq. (11):

$$\frac{m_s c_{p,s} dT}{m_{st} c_{p,st} dT} = \frac{\delta Q_s}{\delta Q_{st}} \quad (11)$$

and:

$$c_{p,s} = c_{p,st} \frac{m_{st}}{m_s} \frac{\delta Q_s}{dt} \frac{dt}{\delta Q_{st}} \quad (12)$$

δQ_{st} is not measured directly but a difference of temperature between the reference and the study crucibles, $DSC_{st}(t) = \Delta T(t)$, is. After the blank correction, it is expressed as $DSC_{st}(t) - DSC_b(t)$. A calibration function $K(T)$, inherent in the device, links δQ_{st} to the measured signal: $\delta Q_{st}/dt = K(T) \cdot (DSC_{st}(t) - DSC_b(t))$. The same is true for δQ_s. Thus Eq. (12) can be expressed as:

$$c_{p,s}(\mathrm{t}) = c_{p,st} \frac{m_{st}}{m_s} \frac{K(T) \cdot (DSC_s(t) - DSC_b(t))}{K(T) \cdot (DSC_{st}(t) - DSC_b(t))} \tag{13}$$

Eventually, after simplifications, the specific heat capacity of the sample $c_{p,s}$ is expressed by Eq. (14):

$$c_{p,s} = c_{p,st} \frac{m_{st}}{m_s} \frac{DSC_s - DSC_b}{DSC_{st} - DSC_b} \tag{14}$$

where $c_{p,st}$ (J.kg^{-1}.K^{-1}) is the specific heat capacity of the sapphire, m_{st} and m_s (g) are the masses of the sapphire and the sample, DSC_{st}, DSC_s and DSC_b (µV) are the DSC signals of the sapphire, the sample and the blank.

The measurements started at ambient temperature. They were performed on 4 samples of hemp shiv and 3 samples of binder.

For the Calvet calorimeter method, a temperature ramp was applied to two cavities surrounded by Tian-Calvet thermopiles, similarly to the DSC approach. These thermopiles measured the heat flux through the cells more precisely. Only a blank and a sample cycle were required in this configuration. During the measurement, the dry sample was put in a closed cell for stabilization at 22 °C and a ramp of temperature was set from 22 °C to 70 °C. Six samples were tested.

The specific heat capacity can be also calculated from the measurement of two thermal properties. The thermal conductivity k ($W.m^{-1}.K^{-1}$) is often one of them and the second one can be, for instance, the thermal effusivity b ($J.m^{-2}.K^{-1}.s^{-½}$):

$$b = \left(k\ \rho\ c_p\right)^{1/2} \tag{15}$$

Knowing the thermal conductivity, the thermal effusivity, and the density, the specific heat capacity c_p is defined by Eq. (16):

$$c_p = \frac{k\ \rho}{b^2} \tag{16}$$

Thermal effusivity is a surface property expressing the ability of a material to transfer heat to another material with which it is in contact: hence the surface temperature will depend on the temperature and the effusivity of both materials.

To measure this parameter, a thermal conductivimeter with a hot plane was used. According to the technical specifications provided by the manufacturer, the accuracy on thermal effusivity is of 5%. The hot plane probe, including a surface resistance and a thermocouple, was placed between two samples (Figure 5).

Based on the works of Carslaw and Jaeger (1959), Jannot (2011) and Krapez (2007), the surface temperature is given by Eq. (17), with the assumption of a semi-infinite material:

$$T(t) = q"\left(R_T - \frac{C_{p,probe}}{(S \cdot b)^2} + \frac{2\sqrt{t}}{b\sqrt{\pi}}\right) \tag{17}$$

where $q"$ is the heat transfer rate ($W.m^{-2}$), R_T is the total thermal resistance (contact resistance + probe resistance) ($m^2.K.W^{-1}$), $C_{p,probe}$ is the heat capacity of the probe ($J.K^{-1}$) and S is the surface area (m^2).

The temperature is then plotted as a function of $\sqrt{t}$. In time, the relation between the two is linear, and the slope is $2/(b\sqrt{\pi})$. The heat rate and test duration were chosen in order to ensure both a sufficient temperature increase (~10 K) and a high correlation coefficient R^2 (>0.999).

A total of twelve measurements were performed on six dry HC samples (25x10x2.5 cm^3).

3. Results and discussion

3.1. Density, porosity and mass ratios

The measurements of the hemp concrete apparent density and the solid densities of the components (Eq. (1)) are presented in Table 2. The calculated total porosity (Eq. (2)) and the open porosity (Eq. (3)), together with the calculated ratios of components (Eq. (4)), are also presented. Table 3 shows some results from the literature concerning the apparent density, solid density and porosities of the HC, hemp shiv and hemp fibre, and also of a lime-metakaolin binder. Despite the numerous studies on the multiphysical characteristics of hemp concrete and their strong link with the material porosity, few porosity values can be found in the literature.

Material	Apparent density ($kg.m^{-3}$)	Solid density ($kg.m^{-3}$)	Total porosity	Open porosity	Mass ratio
	$\rho_{a,HC}$	ρ_i	ε_{tot}	ε_{open}	x_i
HC	466 ±25	2149 ±9	0.78 ±0.04	0.76 ±0.01	-
Hemp shiv	-	1452 ±10	-	-	0.12 ±0.02
Binder	-	2305 ±29	-	-	0.88 ±0.02

Table 2: Density, porosity and mass ratio of the hemp concrete and its components

Material	Apparent density ($kg.m^{-3}$)	Solid density ($kg.m^{-3}$)	Total porosity	Open porosity	Reference
HC	440 ± 20	1660 ± 30	0.73 ± 0.01		(Evrard, 2008)
HC	478 ± 7	2030 ± 30	0.76 ± 0.001	0.50 ± 0.02	(Rahim et al., 2016b)
HC	430-460	1655-2002	0.72-0.79	0.66 - 0.77	(Collet et al., 2013)
HC	508-627	-	-	-	(Walker and Pavía, 2014)
HC	351-410	1211-1537		0.7-0.79	(Gourlay et al., 2017)
Hemp shiv	256.4	1465			(Nguyen et al., 2009)
Hemp shiv (partial defibring)	256.4	1438			
Lime-metakaolin binder	1454-1584	2434-2574	-	-	(Vejmelková et al., 2012)

Table 3: Literature values of HC and its components density and porosity

The literature values show a rather wide range of HC apparent densities, from 430 to 627 $kg.m^{-3}$ (wall configuration) (Collet et al., 2013; Evrard, 2008; Rahim et al., 2016b; Walker and Pavía, 2014). The apparent density of the HC measured here is not far from the average of Table 3, with $\rho_{a,HC} = 466 \pm 25$ $kg.m^{-3}$. The total porosity (0.78) is within the range of the literature values and this porosity is mainly open (0.76) as can be observed in the results of Collet et al. (2013). The HC solid density is slightly higher than the 2030 $kg.m^{-3}$ measured by Rahim et al. (2016b), the 1660 $kg.m^{-3}$ found by Evrard (2008), and the 1655-2002 $kg.m^{-3}$ range given by Collet et al. (2013). The hemp shiv and binder solid density found in the present study are in good agreement with literature values: the first is in the same range as Nguyen et al.'s (2009) values and the second is close to the values measured by Vejmelková et al. (2012).

3.2. **Air permeability**

The experimental results for $k_{p,app}$ (m^2) are presented as a function of ΔP. Figure 8a shows the results for a flow between 20 $mL.min^{-1}$ and 300 $mL.min^{-1}$. We can see a small discrepancy among the measurements: for most measurements (1 Pa<ΔP<6 Pa), the apparent permeability lies between 1 10^{-10} and 1.4 10^{-10} m^2. Values under 1 Pa are expected to increase because of the mathematical expression; they are not considered here. Figure 8b shows the results at higher flow rates, and thus higher pressure differences, from 1 L/min to 2 L/min. As expected, at higher pressure differences, the air permeability is lower, reaching 6 10^{-11} m^2.

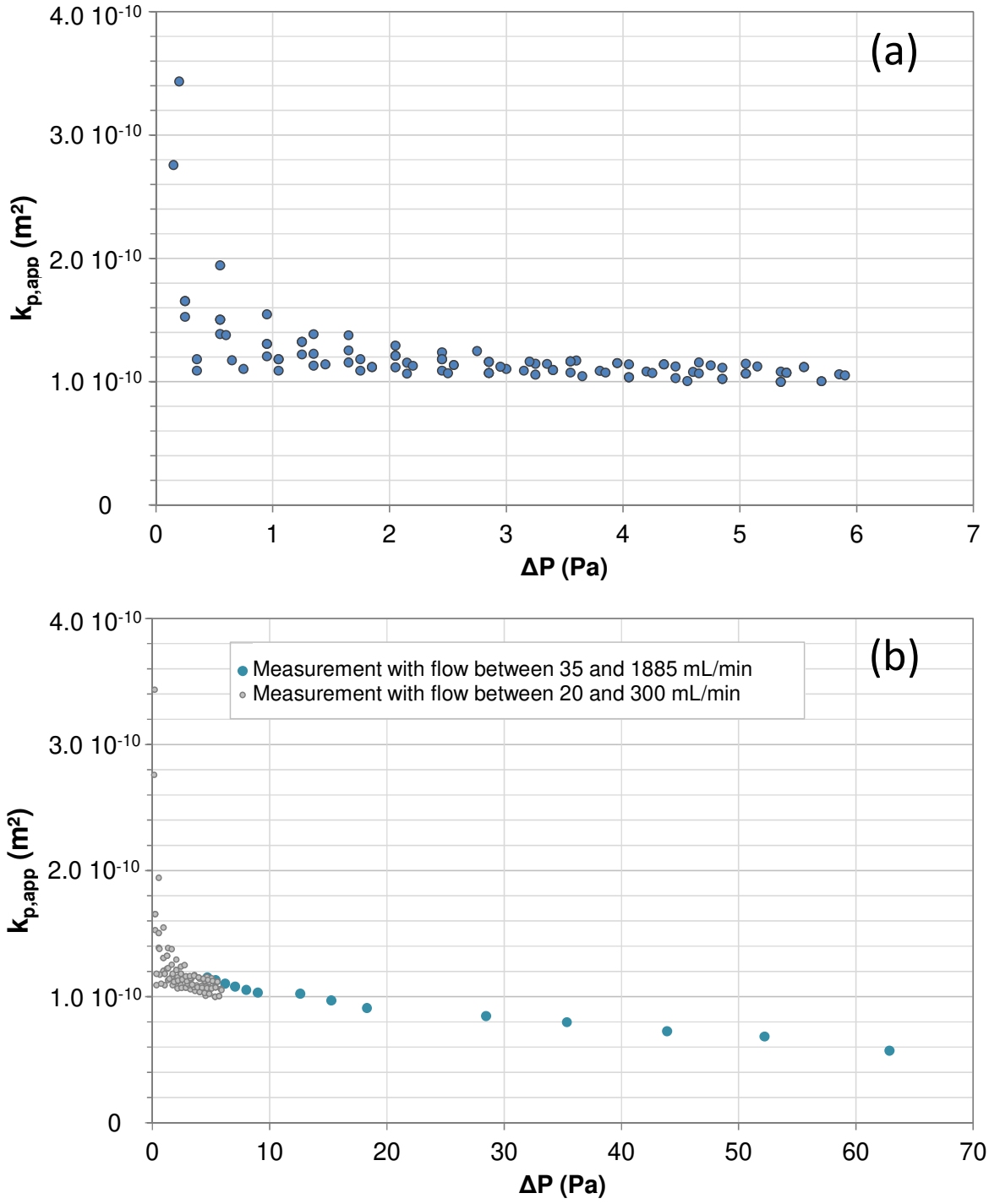

Figure 8: Apparent gas permeability vs ΔP ((a): ΔP range: 0-6 Pa; (b): ΔP range: 0-70 Pa)

With the aim of using a value of air permeability in a numerical model of heat and moisture transfer, we can focus on the results in a range of pressure under about ten pascals, which corresponds to the pressure difference found across a building wall with a wind velocity of up to 4 $m.s^{-1}$. A value of around 10^{-10} m^2 can then be considered.

Glé et al. (2011) studied the acoustic properties of some hemp concretes. Based on the standard ISO 9053, they measured the air flow resistivity, σ (N.s.m^{-4}). Assuming that Darcy's law can be applied, the corresponding air permeability would range from 1.7 10^{-9} to 2.5 10^{-10} m^2 for densities ranging from 390 to 420 kg.m^{-3}.

Hemp concrete is considered as a very permeable construction material. Although ten times less permeable than mineral wool (1.5 10^{-9} m^2 measured by Harreither et al. (2015)), it is far more permeable than other usual construction materials: for instance, Hagentoft (2001) indicated 1.4 10^{-12} m^2 for light weight concrete (ρ=510 kg.m^{-3}) and 4.4 10^{-15} m^2 for concrete in which W/C=0.6, and ρ=2100 kg.m^{-3}, and Wägner et al. (1995) measured 1.0 10^{-14} to 5.5 10^{-13} m^2 for autoclaved aerated concretes (320-700 kg.m^{-3}).

3.3. **Thermal conductivity**

Figure 9 presents the thermal conductivity measured with the hot wire and GHP, compared to measurements from the literature; the main methods used by the different authors are identified by different colours (light blue: hot ring/hot plane, dark blue: hot wire, red: GHP, green: based on hot box) and the uncertainties are indicated when available. Furthermore, some authors distinguish between the case where the heat flux is parallel to the aggregate (identified as "parallel" in the figure) and the case where the heat flux is perpendicular to the aggregate (identified as "perpendicular" in the figure). In our case, the measurement considered the heat flux across the brick in the direction of use. It can thus be identified as "parallel" to the aggregate.

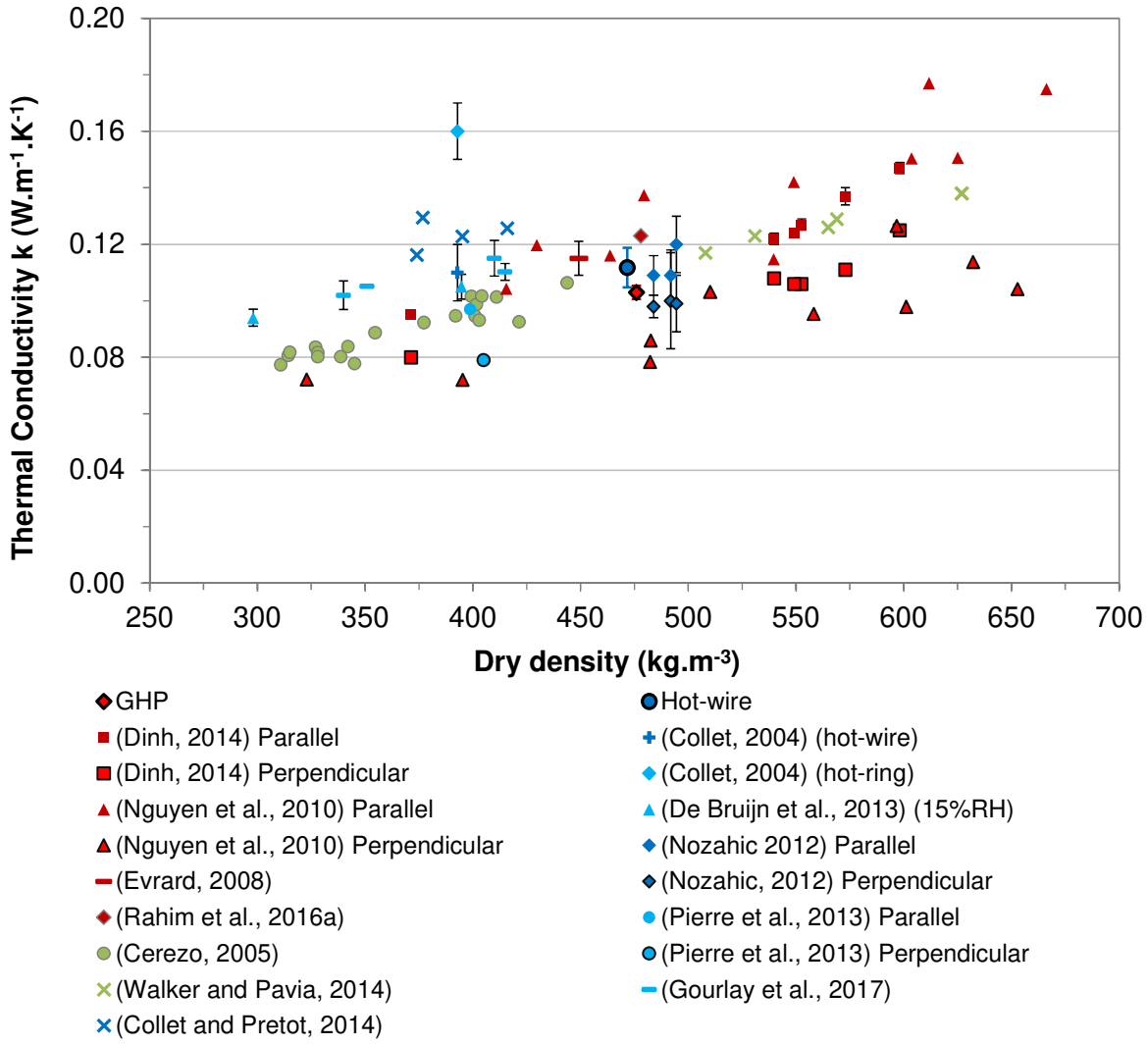

Figure 9: Dry thermal conductivity measured with hot wire and GHP and literature values (light blue: hot ring/hot plane, blue: hot wire, red: GHP, green: based on hot box). The uncertainties are displayed when available)

With GHP measurements, we obtained a mean value of k_{dry}=0.103±0.002 W.m^{-1}.K^{-1} while hot wire measurement led to k_{dry}=0.112±0.007 W.m^{-1}.K^{-1} (around 9% higher). These results are within the range of the literature results for similar dry density. The scatter remains below most of the previously published results with a coefficient of variation of 2.0% and 6.3% for GHP and hot wire methods, respectively. This difference can be partially explained by the prefabrication process, which guarantees consistency of the performances of hemp concrete unlike manual laboratory fabrication, which can lead to some variability.

Thus, the GHP method led to a conductivity value 9% lower than the hot wire one. This difference appears significant considering the experimental dispersion. Nevertheless, on the basis of the literature results presented in Figure 9 (Collet, 2004; Collet and Pretot, 2014; de Bruijn and Johansson, 2013; Dinh, 2014; Evrard, 2008; Gourlay et al., 2017; Nguyen et al., 2010; Nozahic, 2012; Pierre et al., 2014; Rahim et al., 2016a; Walker and Pavía, 2014), no general trend can be observed concerning the impact of the method on the measurement of this parameter.

Figure 10 shows the influence of the temperature on the thermal conductivity. The results show a linear increase of thermal conductivity with the temperature. Between 10 °C and 40 °C, k_{dry} increases by 12%. As observed experimentally in previous studies, a linear relation links the thermal conductivity and the density (Pierre et al., 2014; Rahim et al., 2016a). For our hemp concrete, $k(T)=0.0004T+0.0948$. We can see that the increase of thermal conductivity with the temperature of the studied material is twice as high as measured by Rahim et al. (2016a) and Pierre et al. (2014) in “parallel” configuration but it is close to the result of Pierre et al. (2014) in “perpendicular” configuration.

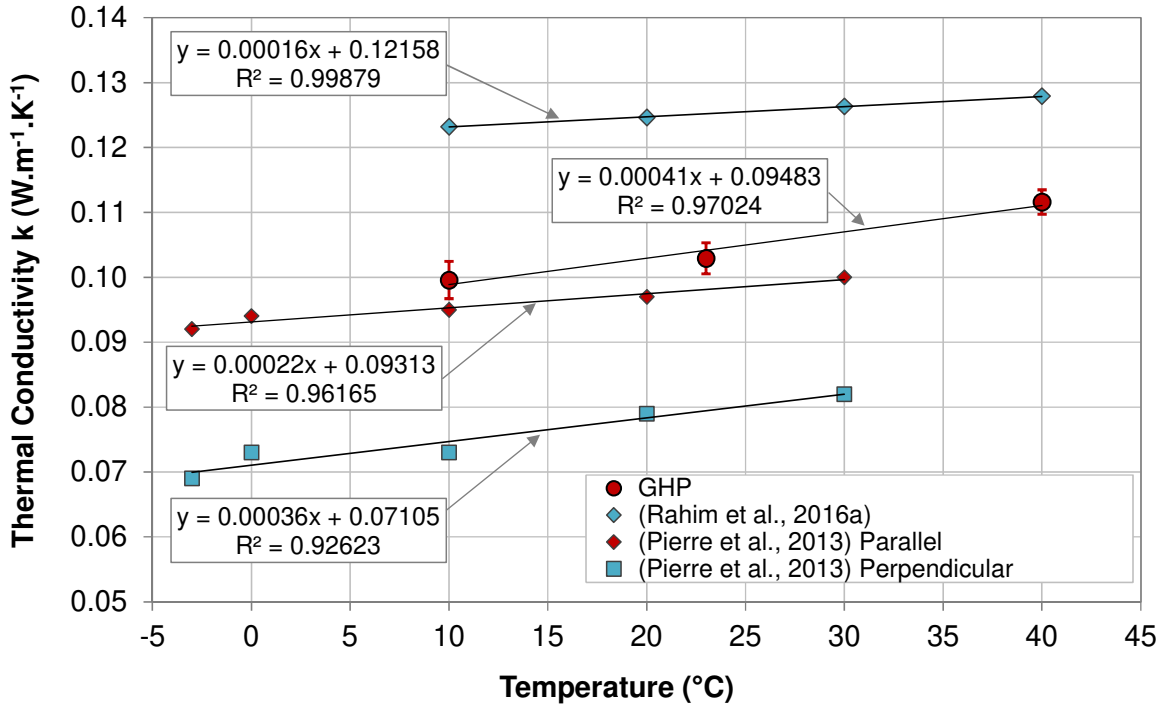

Figure 10: Thermal conductivity as a function of temperature.

Figure 11 shows the thermal conductivity as a function of the humidity, measured with the hot wire device. The self-consistent scheme (SCS) was applied to these experimental results. This homogenization model, commonly used on building materials and hemp concrete (Boutin,1996; Collet, 2014a; Rahim, 2016a), evaluates the effective thermal conductivity of a heterogeneous material, i.e. with different phases such as air (a), water (w) and solid phases (s). It is based on the assumption of a concentric spherical inclusion with radius R for each phase (Figure 12).

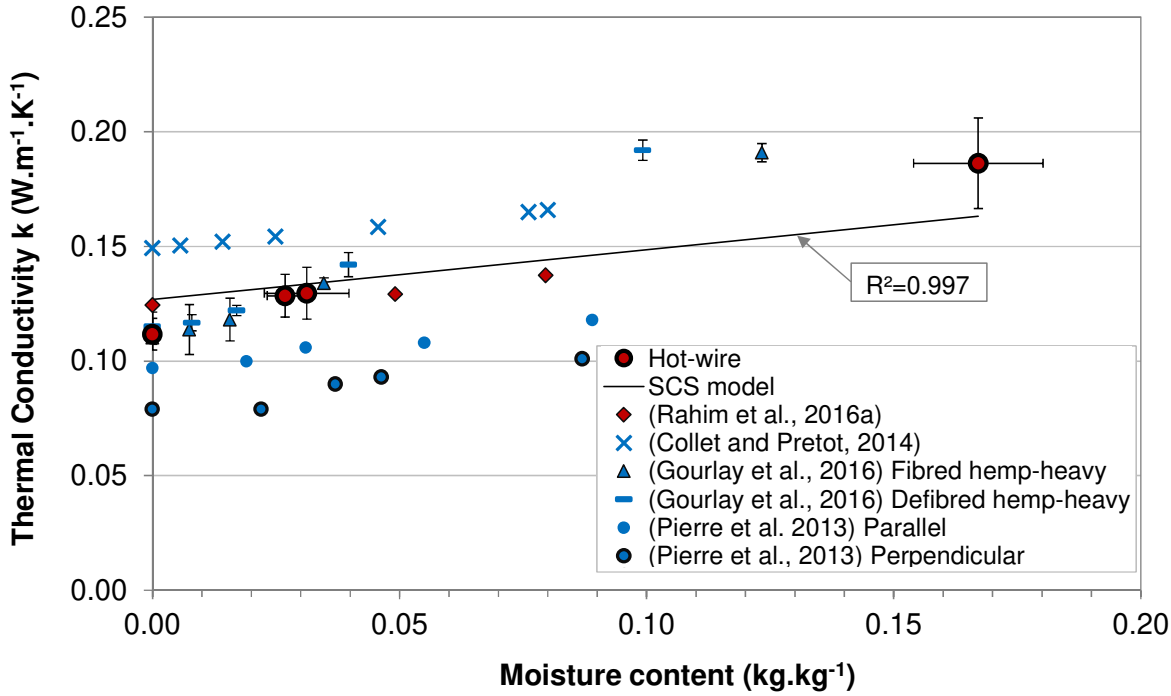

Figure 11: Thermal conductivity as a function of moisture content (experimental value and SCS model)

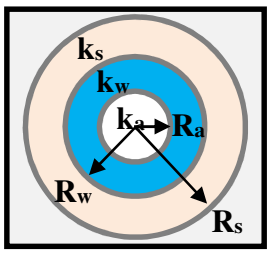

Figure 12: Three phase composite sphere in self-consistent model (Boutin, 1996).

The resulting expression of the SCS model is:

$$k_{eq} = k_s \left(1 + \frac{\varepsilon}{\left(\frac{1-\varepsilon}{3} + \frac{3 + \delta(k_a/k_w - 1)}{3(k_a/k_s - 1) - \delta(k_a/k_w - 1)(2\,k_w/k_s + 1)} \right)} \right) \qquad (18)$$

where ε is the porosity and $\delta = u \cdot \rho_{a,HC}/(\rho_w\, \varepsilon\,)$, with u (kg/kg) the moisture content, $\rho_{a,HC}$ the apparent hemp concrete density (kg.m^{-3}) and ρ_w the water density (kg.m^{-3}). The solid thermal conductivity, k_s, is found by fitting the model to the experimental values using the least squares method.

The resulting expression for the equivalent thermal conductivity of the hemp concrete is:

$$k_{eq}(\mathrm{u}) = 0.224\mathrm{u} + 0.132 \quad (19)$$

There was good agreement with literature values: Collet and Pretot (2014) and Rahim et al. (2016a) found, according to the SCS model, k(u)=0.208·u+0.149 and k(u)=0.258·u+0.126, respectively.

3.4. **Specific heat capacity**

The specific heat capacity of the hemp shiv and the lime-metakaolin binder are presented in Figure 13 as functions of the temperature measured with the DSC device (mean value ± standard deviation for our measurements).

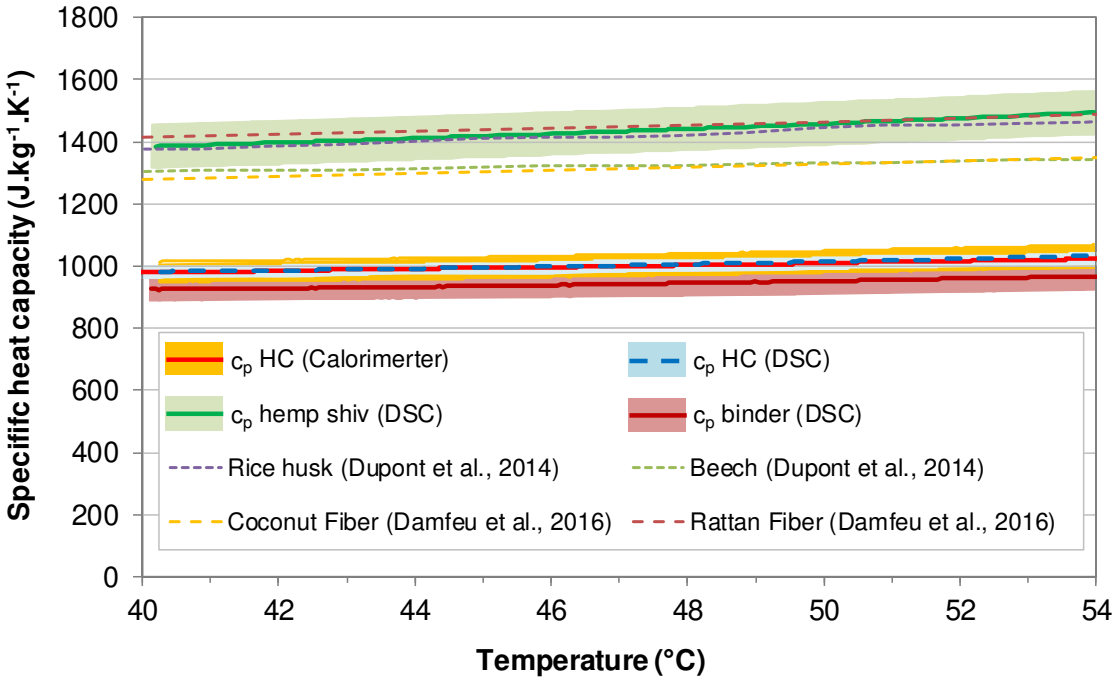

Figure 13: Hemp and binder c_p measured with DSC and resulting HC c_p as a function of the temperature, compared to results for various biomasses, and HC c_p measured with a Calvet calorimeter.

Both curves appear linear in the study temperature range (R^2=0.99). Extrapolating the value of hemp specific heat capacity linearly to 23 °C leads to $c_{p,hemp}$=1247±62 J.kg^{-1}.K^{-1}, which is

close to the results found by Bourdot et al. (2017), who measured it as 1272 and 1276 J.kg^{-1}.K^{-1} at 23°C with a Calvet calorimeter for two ranges of size of hemp shiv particles. Values for other biomasses from the literature are also presented (Damfeu et al., 2016; Dupont et al., 2014) and are also close to the DSC measurements. Extrapolating the specific heat capacity of the lime-metakaolin binder linearly to 20 °C leads to $c_{p,binder}$= 859±31 J.kg^{-1}.K^{-1}, which is similar to the values around 900 J.kg^{-1}.K^{-1} obtained for some lime-metakaolin plasters by Vejmelková et al. (2011). As observed in the literature references, the c_p increases linearly with temperature (Damfeu et al., 2016; Dupont et al., 2014). However, this increase seems slightly higher for our hemp shiv measurement.

From the component heat capacity, it is possible to evaluate the heat capacity of the hemp concrete as a whole:

$$c_{p,HC}^{dry} = x_{hemp} c_{p,hemp} + x_{binder} c_{p,binder} \quad (20)$$

Figure 13 also compares the resulting HC specific heat capacity calculated according to Eq. (20) (x_{hemp}=0.12 and x_{binder}=0.88), from the DSC measurements, and with HC c_p measured using the Calvet calorimeter. We can see that both methods give results in the same range of values.

Assuming a linear behaviour of the specific heat capacity, a linear regression from the DSC and calorimeter measurements gave the value at 20°C: $c_{p,HC(DSC)}^{dry}$= 905±44 J.kg^{-1}.K^{-1} and $c_{p,HC(calorimeter)}^{dry}$= 911±17 J.kg^{-1}.K^{-1} which are relatively close values.

The measured effusivity was b=197±16 J.m^{-2}.K^{-1}.s$^{-1/2}$. Very few measurements of the hemp concrete effusivity are available: Collet (2004), Evrard (2008), and Rahim et al. (2016) found respectively 231, 297 and 256 J.m^{-2}.K^{-1}.s$^{-1/2}$ with respective densities of 440, 440 and 478 kg.m^{-3}. Knowing the dry thermal conductivity of our material, k_{dry} = 0.112±0.007 W.m^{-1}.K^{-1}

and the apparent density $\rho_{a,HC}$ = 466±25 kg.m^{-3}, the specific heat capacity was calculated according to Eq. (15): $c_{p,HC(hot\ plane)}^{dry}$ = 741±104 J.kg^{-1}.K^{-1}, assuming the measurements were performed at 20 °C. The measurements of the hemp concrete specific heat capacity with the three types of apparatus are presented in Figure 14, together with the literature values.

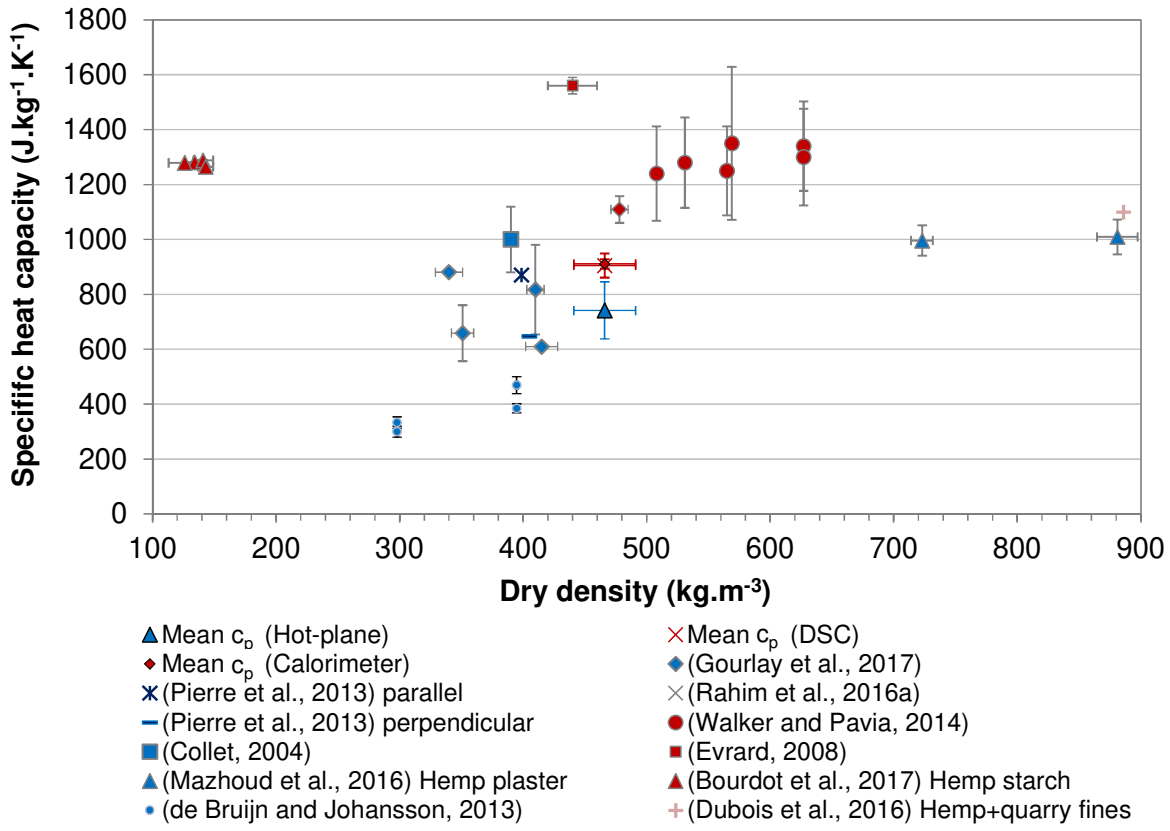

Figure 14: Dry specific heat capacity of hemp concrete measured with DSC, Calvet calorimeter and by means of a hot plane, versus dry density. Literature values are provided for comparison (red: direct measurement, blue: indirect measurement).

From our results, we can see that the method of measurement can significantly impact the final value: although the specific heat capacity measured with the DSC and the Calvet calorimeter are close, the c_p calculated from the hot plane measurement is around 18% lower. This difference can also be explained by the fact that the calculation method relies on the thermal conductivity and density values (Eq. (15)), with their associated uncertainties. This

trend seems to appear in the literature: from the values plotted in Figure 14 (the uncertainties are plotted when available), most c_p values resulting from indirect measurements, generally from calculations based on thermal conductivity and thermal diffusivity measurements, tend to be lower (Collet, 2004; de Bruijn and Johansson, 2013; Gourlay et al., 2017; Mazhoud et al., 2016; Pierre et al., 2014). In contrast, the measurements performed with adiabatic calorimeters (Evrard, 2008; Walker and Pavía, 2014) or the Calvet calorimeter (Bourdot et al., 2017) appear to be higher, whatever the level of density. However, part of the large scatter of the specific heat capacities of hemp concrete, between 300 and 1560 $J.kg^{-1}.K^{-1}$ could be due to the composition. To the best of our knowledge, except in the present paper, there is no comparison of different measurement techniques on the same material. Nevertheless, it can be noted that the results of Pierre et al. (2013) highlight the impact of the anisotropy with indirect measurements: they performed their measurements so that the hemp particles were parallel to the heat flux in one case and perpendicular to it in another. When the hemp shiv aggregates were parallel to the axis of the heat flux, the calculated c_p was 34% higher than in the other configuration. By looking into the details, we thus see that the thermal conductivity k, is 19% higher while the thermal diffusivity a, is only 8% lower - and this explains the difference, since $c_p=k/(\rho.a)$. Thus, the indirect evaluation of the specific heat capacity can be sensitive to the anisotropy of the material. From the same point of view, we can also wonder how the local measurements, such as made with hot wire and hot plane instruments, are affected by the heterogeneity of the material (large pores for instance), typically found in hemp concrete. Despite these observations, the indirect methods are easy and relatively quick to perform with a wide variety of materials. As regards the DSC, this alternative method enables the specific heat capacity of a material to be evaluated by considering its components. It can be as accurate as direct calorimetric measurement but requires the composition of the material under study.

With the dry specific heat capacity of hemp concrete, it is possible to calculate the specific heat capacity as a function of the moisture content (Eq. (21)). The resulting curves are plotted in Figure 15.

$$c_{p,HC} = \left(\frac{1}{1+u}\right) c_{p,HC}^{dry} + \left(\frac{u}{1+u}\right) c_{p,water} \quad (21)$$

where $c_{p,water}$ is the specific heat capacity of water ($c_{p,water}$ = 4187 J.kg^{-1}.K^{-1}).

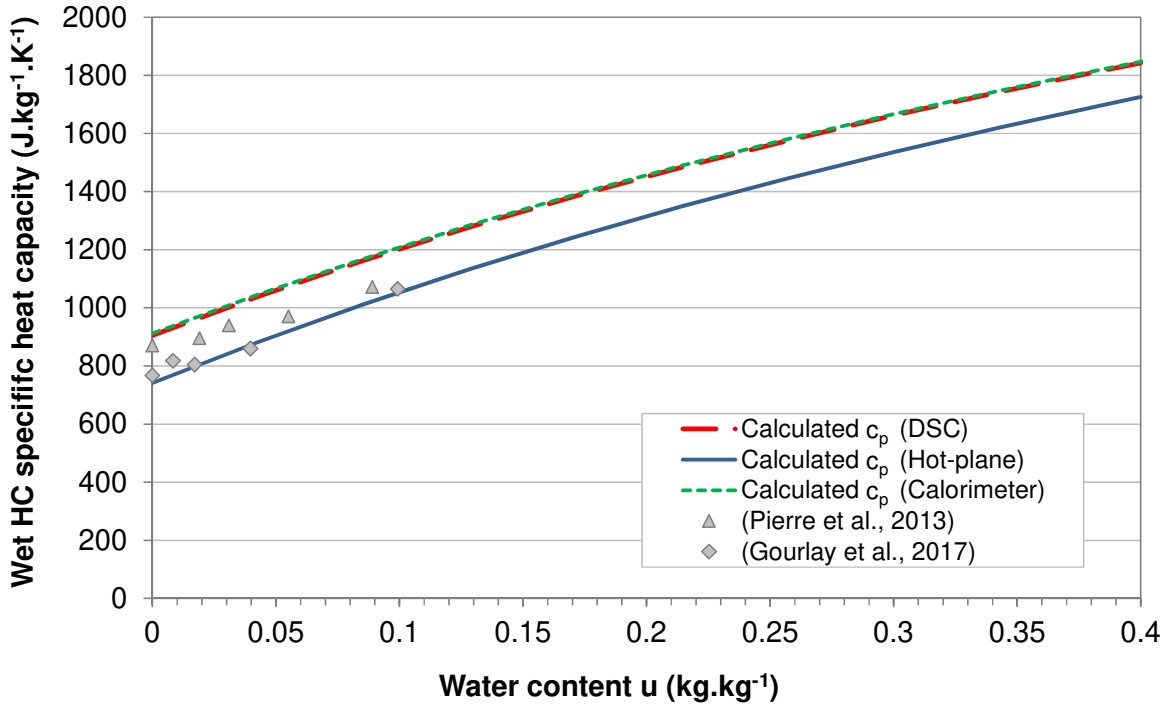

Figure 15: Calculated hemp concrete specific heat capacity and some literature values versus water content.

We can see that the increase of c_p according to the moisture content follows the general trend found by Gourlay et al. (2016) and Pierre et al. (2013), although our values have a slightly greater increase than those of Pierre et al. (2013).

In the heat and moisture model literature, the temperature dependence of the specific heat capacity is neglected. However, the moist material state is taken into account as the heat and moisture model are generally multiphase.

Based on the temperature dependent specific heat capacity of the hemp concrete (Figure 13) and the expression for the specific heat capacity of the moist material (Eq. (21)), a rough approximation of the hemp concrete specific heat capacity as a function of the temperature and moisture content is presented in Figure 16. From this observation, we can state that the influence of moisture content is dominant compared to that of temperature.

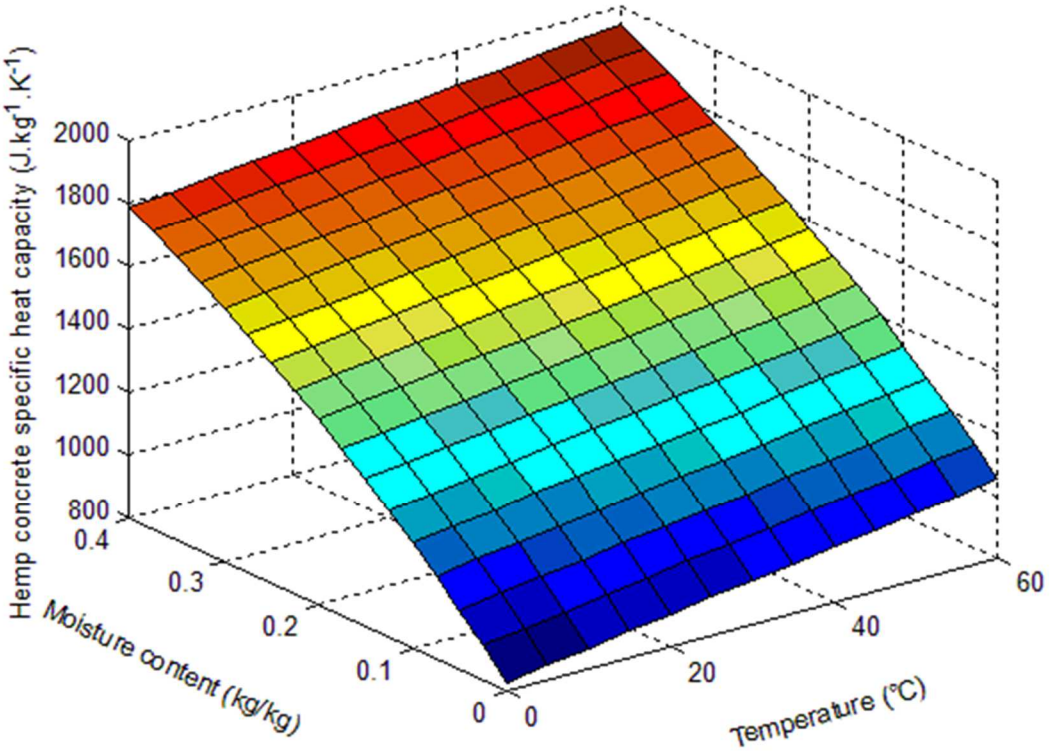

Figure 16: Calculated specific heat capacity of hemp concrete as a function of the moisture content and the temperature

4. Conclusion and prospects

This paper has characterized the physical properties, the air permeability and the thermal properties of a precast hemp concrete.

For the physical properties, the measurement of the density, and the open and total porosity show that the precast hemp concrete studied has a medium density (466 $kg.m^{-3}$) relative to other hemp concretes of the literature. Its high porosity (78%) is almost entirely interconnected (76%).

The gas permeability has rarely been studied in previous work on hemp concrete. The present study allows a measurement method, initially intended for regular concrete, to be adapted to the specific properties of hemp concrete. The measured air permeability leads to the conclusion that it is a very permeable material: for a difference of pressure of around ten pascals, the air permeability of precast hemp concrete is 1.10^{-10} m^2.

For the thermal properties, the thermal conductivity and the specific heat capacity were measured. Different methods were used and confronted on the same material. The thermal conductivity was measured with a guarded hot plate (k_{dry}=0.103±0.002 $W.m^{-1}.K^{-1}$) and a hot wire (k_{dry}=0.112±0.007 $W.m^{-1}.K^{-1}$); the second method led to a value 9% higher, although close to one method uncertainty. Even when an extensive literature comparison was included, no general tendency could be drawn for any method.

The dependence of the dry thermal conductivity on the temperature was assessed experimentally. Concerning the impact of moisture on the thermal conductivity, the experimental data were fitted with the SCS scheme.

The specific heat capacity was measured with two direct measurements, differential scanning calorimetry and a Calvet calorimeter, and with one indirect method relying on the effusivity measurement, which required additional measurements of thermal conductivity and density.

The proposed method using DSC was based on the measurement of the specific heat capacity of each component (hemp shiv and pozzolanic binder). This method was shown to be as accurate as direct calorimetric measurement.

The two direct measurements gave the same result (905 and 911 $J.kg^{-1}.K^{-1}$), while the indirect measurement led to a result 18% lower for the dry value. A comprehensive analysis of the measurement values available in the literature on hemp concretes confirmed this trend. From the DSC measurement of the dry specific heat capacity as a function of the temperature, it was possible to calculate the moist hemp concrete specific heat capacity.

This first paper highlights the significant influence of the testing method on the determination of the thermal properties of a precast hemp concrete, especially on the heat capacity measurement. This result emphasizes the need for a large inter-laboratory experimental campaign, applied to bio-aggregate based concrete, in order to form the basis of recommendations for adequate physical and thermal characterization methods for these bio-based building materials.

The second paper of this series focuses on the hydric properties of the same precast hemp concrete with a similar approach of confronting different test methods for sorption isotherm, water vapour permeability and liquid permeability determination. All these experimental values will be used as input for modelling heat and moisture transfers. These numerical results will then be confronted with measurements made on a wall-scale set-up.

5. Acknowledgments

The authors would like to acknowledge the SEAC company, which provided the materials for this study, and the scientific project neOCampus, led by Paul Sabatier University Toulouse III, which supports this work.

References

AFNOR, 2016. NF EN ISO 11357-1:2016 - Plastics — Differential scanning calorimetry (DSC) — Part 1: General principles.

AFNOR, 2014. NF EN ISO 11357-4:2014 - Plastics — Differential scanning calorimetry (DSC) — Part 4: Determination of specific heat capacity.

AFNOR, 2001. NF EN 12664 - Thermal performance of building materials and products - Determination of thermal resistance by means of guarded hot plate and heat flow meter methods - Dry and moist products of medium and low thermal resistance.

AFPC-AFREM, 1997. Recommended Method for Durability Indicator, in: Proceedings of Technical Meeting AFPC–AFREM. Toulouse, France.

Aitcin, P.C., Garnier, G., Carles Gibergues, A., 1968. Powder density measurement by hydrostatic weighing. American Mineralogist 53, 1413–1417.

Arnaud, L., Gourlay, E., 2012. Experimental study of parameters influencing mechanical properties of hemp concretes. Construction and Building Materials 28, 50–56.

Association Construire en chanvre, Collectif FFB, 2007. Construire en chanvre - Règles professionnelles. SEBTP.

ASTM, 2011. ASTM 1269-Standard Test Method for Determining Specific Heat Capacity by Differential Scanning Calorimetry.

Benfratello, S., Capitano, C., Peri, G., Rizzo, G., Scaccianoce, G., Sorrentino, G., 2013. Thermal and structural properties of a hemp–lime biocomposite. Construction and Building Materials 48, 745–754.

Blengini, G.A., Di Carlo, T., 2010. The changing role of life cycle phases, subsystems and materials in the LCA of low energy buildings. Energy and Buildings 42, 869–880.

Bourdot, A., Moussa, T., Gacoin, A., Maalouf, C., Vazquez, P., Thomachot-Schneider, C., Bliard, C., Merabtine, A., Lachi, M., Douzane, O., Karaky, H., Polidori, G., 2017. Characterization of a hemp-based agro-material: Influence of starch ratio and hemp shive size on physical, mechanical, and hygrothermal properties. Energy and Buildings 153, 501–512.

Boutin, C., 1996. Conductivité thermique du béton cellulaire autoclavé: modélisation par méthode autocohérente. Mat. Struct. 29, 609–615.

Buyle, M., Braet, J., Audenaert, A., 2013. Life cycle assessment in the construction sector: A review. Renewable and Sustainable Energy Reviews 26, 379–388.

Carslaw, H.S., Jaeger, J.C., 1959. Conduction of heat in solids. Clarendon Press.

Cembureau Recommendation, 1989. The Determination of the Permeability of Concrete to Oxygen by the Cembureau Method.

Cerezo, V., 2005. Propriétés mécaniques, thermiques et acoustiques d'un matériau à base de particules végétales: approche expérimentale et modélisation théorique (Ph.D. thesis). Ecole Nationale des Travaux Publics de l'Etat (ENTPE).

Collet, F., 2004. Caractérisation hydrique et thermique de matériaux de génie civil à faibles impacts environnementaux (Ph.D. thesis). INSA de Rennes.

Collet, F., Chamoin, J., Pretot, S., Lanos, C., 2013. Comparison of the hygric behaviour of three hemp concretes. Energy and Buildings 62, 294–303.

Collet, F., Pretot, S., 2014. Thermal conductivity of hemp concretes: Variation with formulation, density and water content. Construction and Building Materials 65, 612–619.

Damfeu, J.C., Meukam, P., Jannot, Y., 2016. Modeling and measuring of the thermal properties of insulating vegetable fibers by the asymmetrical hot plate method and the radial flux method: Kapok, coconut, groundnut shell fiber and rattan. Thermochimica Acta 630, 64–77.

de Bruijn, P., Johansson, P., 2013. Moisture fixation and thermal properties of lime–hemp concrete. Construction and Building Materials 47, 1235–1242.
Delgado, J.M.P.Q., Barreira, E., Ramos, N.M.M., de Freitas, V.P., 2013. Hygrothermal Numerical Simulation Tools Applied to Building Physics, Springer Briefs in Applied Sciences and Technology. Springer Berlin Heidelberg, Berlin, Heidelberg.
Dinh, T.M., 2014. Contribution to the development of precast hempcrete using innovative pozzolanic binder (Ph.D. thesis). Université Toulouse 3 Paul Sabatier.
Dinh, T.M., Magniont, C., Coutand, M., Escadeillas, G., 2015. Hemp concrete using innovative pozzolanic binder. Presented at the First International Conference on Bio-based Building Materials.
Dupont, C., Chiriac, R., Gauthier, G., Toche, F., 2014. Heat capacity measurements of various biomass types and pyrolysis residues. Fuel 115, 644–651.
Escadeillas, G., Oms, C., Magniont, C., De, C.P., 2010. Binder composition, useful for forming construction materials, comprises natural lime binder, metakaolin binder, and binder of an adjuvant comprising shrinkage reducer, water repellent hardener. FR2946641 (A1).
Evrard, A., 2008. Transient hygrothermal behaviour of Lime-Hemp Materials (Ph.D. thesis). Université Catholique de Louvain.
Fang, L., Clausen, G., Fanger, P.., 1998. Impact of temperature and humidity on the perception of indoor air quality. Indoor Air 8, 80–90.
Gazagnes, E., Magniont, C., Escadeillas, G., 2010. Composite material for construction comprising hemp stems. FR2946640 (A1) Abrégé du document correspondant EP2263985 (A1).
Glé, P., Gourdon, E., Arnaud, L., 2011. Acoustical properties of materials made of vegetable particles with several scales of porosity. Applied Acoustics 72, 249–259.
Glouannec, P., Chauvelon, P., Colinart, T., Le Bideau, P., Zaknoune, A., Jameladine, N., 2010. Experimental and numerical studies of the drying of hemp concrete, in: 17th International Drying Symposium (IDS 2010). Magdeburg, Germany, pp. 2028–2033.
Gourlay, E., Glé, P., Marceau, S., Foy, C., Moscardelli, S., 2017. Effect of water content on the acoustical and thermal properties of hemp concretes. Construction and Building Materials 139, 513–523.
Gradeci, K., Labonnote, N., Time, B., Köhler, J., 2017. Mould growth criteria and design avoidance approaches in wood-based materials – A systematic review. Construction and Building Materials 150, 77–88.
Hagentoft, C.-E., 2001. Introduction to Building Physics. Studentlitteratur AB, Lund.
Harreither, C., Krainz, L., Weissinger, J., Bednar, T., 2015. Experimental Determination of the Influence of Installing Fibrous Insulation Materials in Timber Frames on the Air Permeability and Convective Air Transport. Energy Procedia, 6th International Building Physics Conference, IBPC 2015 78, 2748–2753.
Jannot, Y., 2011. Théorie et pratique de la métrologie thermique. LEMTA, Université de Nancy.
Jones, D., Brischke, C., 2017. Performance of Bio-based Building Materials. Woodhead Publishing.
Krapez, J.-C., 2007. Mesure de l'effusivité thermique Méthodes par contact. Techniques de l'ingénieur Mesure des grandeurs thermophysiques base documentaire : TIB544DUO.
Latha, P.K., Darshana, Y., Venugopal, V., 2015. Role of building material in thermal comfort in tropical climates – A review. Journal of Building Engineering 3, 104–113.
Magniont, C., Escadeillas, G., Coutand, M., Oms-Multon, C., 2012. Use of plant aggregates in building ecomaterials. European Journal of Environmental and Civil Engineering 16, 17–33.

Mazhoud, B., Collet, F., Pretot, S., Chamoin, J., 2016. Hygric and thermal properties of hemp-lime plasters. Building and Environment 96, 206–216.

Ministère de la transition écologique et solidaire, Ministère de la cohésion des territoires, 2017. Référentiel « Energie-Carbone » pour les bâtiments neufs - Méthode d'évaluation de la performance énergétique et environnementale des bâtiments neufs.

Nguyen, T.-T., Picandet, V., Amziane, S., Baley, C., 2009. Influence of compactness and hemp hurd characteristics on the mechanical properties of lime and hemp concrete. European Journal of Environmental and Civil Engineering 13, 1039–1050.

Nguyen, T.T., Picandet, V., Carre, P., Lecompte, T., Amziane, S., Baley, C., 2010. Effect of compaction on mechanical and thermal properties of hemp concrete. European Journal of Environmental and Civil Engineering 14, 545–560.

Nozahic, V., 2012. Vers une nouvelle démarche de conception des bétons de végétaux lignocellulosiques basée sur la compréhension et l'amélioration de l'interface liant/végétal - Application à des granulats de chènevotte et de tige de tournesol associés à un liant ponce/chaux (Ph.D. thesis). Université Blaise Pascal - Clermont II.

Pierre, T., Colinart, T., Glouannec, P., 2014. Measurement of Thermal Properties of Biosourced Building Materials. Int J Thermophys 35, 1832–1852.

Plagge, R., Scheffler, G., Nicolai, A., 2007. Experimental Methods to Derive Hygrothermal Material Functions for Numerical Simulation Tools. Presented at the Buildings X : Thermal Performance of the Exterior Envelopes of Whole Buildings.

Rahim, M., Douzane, O., Tran Le, A.D., Langlet, T., 2016a. Effect of moisture and temperature on thermal properties of three bio-based materials. Construction and Building Materials 111, 119–127.

Rahim, M., Douzane, O., Tran Le, A.D., Promis, G., Langlet, T., 2016b. Characterization and comparison of hygric properties of rape straw concrete and hemp concrete. Construction and Building Materials 102, Part 1, 679–687.

Rahim, M., Tran Le, A.D., Douzane, O., Promis, G., Langlet, T., 2016c. Numerical investigation of the effect of non-isotherme sorption characteristics on hygrothermal behavior of two bio-based building walls. Journal of Building Engineering 7, 263–272.

Seng, B., Lorente, S., Magniont, C., 2017. Scale analysis of heat and moisture transfer through bio-based materials — Application to hemp concrete. Energy and Buildings 155, 546–558.

Service de l'observation et des statistiques (SOeS), 2017. Chiffres clés de l'environnement - Parte 1-Milieux naturels et biodiversités: état, pressions - Emissions des gaz à effet de serre par secteur [WWW Document]. Ministère de la transition écologique et solidaire - Commissariat général au Développement durable - Observation et statistiques. URL http://www.statistiques.developpement-durable.gouv.fr/indicateurs-indices/f/2082/0/emissions-gaz-effet-serre-secteur-1.html (accessed 9.11.17).

Service de l'observation et des statistiques (SOeS), 2016. Chiffres clés de l'énergie (No. Edition 2015). Commissariat général au développement durable.

Shea, A., Lawrence, M., Walker, P., 2012. Hygrothermal performance of an experimental hemp–lime building. Construction and Building Materials 36, 270–275.

Vejmelková, E., Keppert, M., Máca, P., Černý, R., 2011. Mechanical, hygric and thermal properties of innovative renovation renders. pp. 555–563.

Vejmelková, E., Koňáková, D., Čáchová, M., Keppert, M., Černý, R., 2012. Effect of hydrophobization on the properties of lime–metakaolin plasters. Construction and Building Materials, Non Destructive Techniques for Assessment of Concrete 37, 556–561.

Viitanen, H., Vinha, J., Salminen, K., Ojanen, T., Peuhkuri, R., Paajanen, L., Lähdesmäki, K., 2010. Moisture and Bio-deterioration Risk of Building Materials and Structures. Journal of Building Physics 33, 201–224.

Vu, T.L., Spagnol, S., Magniont, C., 2015. Experimental study of the hygrothermal behaviour of hemp shives-based precast blocks at material and wall scales. Presented at the First International Conference on Bio-based Building Materials (ICBBM), Clermont-Ferrand, France.

Wägner, F., Schober, G., Mörtel, H., 1995. Measurement of the gas permeability of autoclaved aerated concrete in conjunction with its physical properties. Cement and Concrete Research 25, 1621–1626.

Walker, R., Pavía, S., 2014. Moisture transfer and thermal properties of hemp–lime concretes. Construction and Building Materials 64, 270–276.

Walker, R., Pavía, S., 2012. Impact of water retainers in the strength, drying and setting of lime hemp concrete. Presented at the Bridge and Concrete Research in Ireland (BCRI), Dublin.